Developing Photo-Activable Ruthenium (II) Complexes for PDT: Synthesis, Characterization, Photophysical and Biological Studies

Clara Parella,[a] Andreu Blanquer,[b] Sohini Sinha,[c] Evelyn Hümpfner,[d] Jordi Hernando,[e] Eloi Mora,[a] Xavier Fontrodona,[a] Zsolt Kelemen,[d] Carme Nogués,[b] Rosario Núñez,[c*] and Isabel Romero[a*]

[a]*Departament de Química and Serveis Tècnics de Recerca, Universitat de Girona, C/ M. Aurèlia Campmany, 69, E-17003 Girona, Spain.* marisa.romero@udg.edu

[b]*Departament de Biologia Cellular, Fisiología i Immunologia, Universitat Autònoma de Barcelona, E-08193 Bellaterra, Barcelona, Spain.*

[c]*Institut de Ciència de Materials de Barcelona, ICMAB-CSIC, Campus UAB, E-08193 Bellaterra, Spain.* rosario@icmab.es

[d] *Department of Inorganic and Analytical Chemistry, Budapest University of Technology and Economics, Műegyetem RKP 3 H-1111 Budapest, Hungary.*

[e]*Departament de Química. Universitat Autònoma de Barcelona, E-08193 Bellaterra (Barcelona), Spain.*

ABSTRACT

The easy tunable photophysical properties of Ru(II) polypyridyl complexes, together with their water solubility, photochemical stability and high biocompatibility make them suitable as agents for photodynamic therapy (PDT). The development of complexes containing new ligands is a step forward in the improvement and application of these compounds as photosensitizer and photocytotoxic agents. We report the synthesis of a set of Ru(II)-polypyridyl complexes with different electronic properties and delocalized π systems: one homoleptic complex $[Ru^{II}(dpbpy)_3](PF_6)_2$ (**1**), and three heteroleptic complexes $[Ru^{II}(dpbpy)_2(phen)](PF_6)_2$ (**2**), $[Ru^{II}(dpbpy)(phen)_2](PF_6)_2$ (**3**) and $[Ru^{II}(dpbpy)_2(CN-Me)](PF_6)_2$ (**4**). All of them contain 4,4'-diphenyl-2,2'-bipyridine (*dpbpy*) and 1,10-phenantroline (*phen*) or N-methyl-N'-2-pyridilimidazolium (CN-Me) ligands. The complexes have been characterized by spectroscopic, structural and electrochemical methods. UV-vis absorption in solution show the red shift for the metal to ligand charge transfer (MLCT) transitions after changing *phen* by *dpbpy* and CN-Me carbene ligands. The photoluminescence emission spectra of **1-4** supported by theoretical calculations using time-dependent density-functional theory (TDDFT) suggest that the lowest energy excited state is mainly ^{3}MLCT. Complex **2** exhibits the highest phosphorescence emission with a quantum yield (Φ_P) in CH_2Cl_2 of 44.1%, followed by complex **1** ($\Phi_P = 40.0\%$), whereas complex **4** shows the lowest quantum efficiency ($\Phi_P = 16.0\%$), what suggest that the introduction of the CN-Me carbene ligand produces a significant quenching of the phosphorescence. Phosphorescence triplet state lifetimes between 0.96 and 1.74 μs were shown for **1-4** in degassed CH_2Cl_2. The trend in the redox potentials becomes more positive by increasing the number of *phen* ligands in the complexes, in full agreement with the HOMO's energy level and the blue shift of the MLCT transitions in the absorption spectra. Complexes internalization was analysed in tumorigenic mammary epithelial SKBR-3 cells, being complexes **1** and **2** the most well internalized. The effect of the photodynamic treatment using light-activated complexes **1** and **2** for 10 min demonstrated to increase cell death, being the homoleptic complex **1** an outstanding candidate as potential theranostic agent for bioimaging and PDT.

INTRODUCTION

Photodynamic therapy (PDT) is a cancer treatment that uses a photosensitizer agent (PS) capable of killing cancer cells using a special type of light.[1] A photosensitizer must fulfil a list of requirements to be a good PDT agent: (1) large molar extinction coefficient (2) effective $^1O_2$ generation, (3) selective accumulation in tumour cells, (4) amphiphilic structure, (5) no dark toxicity and (6) solubility in injectable formulations. In the PDT the photosensitizer generates cytotoxic reactive oxygen (ROS) after activation with light at a specific wavelength in the presence of molecular oxygen ($^3O_2$). When the photosensitizer is internalized in the cell the generation of ROS leads to significant cell damage and eventually cell death.[2,3,4.] Some of the most promising PSs are phorphyrinoids (porphyrins and phtalocyanines),[5,6] however they have important limitations as PSs: on the one hand its main absorption band locates in the ultraviolet–visible (UV–vis), and on the other hand its tendency to aggregate in culture medium through π-π stacking interactions leads to the quenching of their excited states and, consequently, the decrease of their ability to produce $^1O_2$. Then, great efforts have been devoted to design and synthesize new PSs with maxima absorption at higher wavelengths, i.e red and near-infrared (NIR) light-triggered PSs, because these sources of light can afford greater penetration depths and lower phototoxicity to normal tissues than UV and visible light.[7] Another type of PSs includes metal-organic frameworks (MOFs)[8] and metal complexes,[1,9,10,11,12,13] among others.

Owing to their attractive photophysical properties, Ru(II) polypyridyl complexes have been studied and applied in a large number of different applications, such as photocatalysis,[14,15] solar energy conversion,[16] luminescence biological imaging[17] and photodynamic therapeutic applications.[18,19,20] Apart from their outstanding photophysical behaviour, these kind of complexes show excellent biological properties as water solubility, high biocompatibility and photochemical stability, large Stokes shifts, great $^1O_2$ production quantum yield and low toxicity in the dark, making them suitable agents for PDT.[21,22,23,24,25,26]

As previously mentioned, the use of lower energy light is desired in PDT treatments since it allows a better introduction into the tissues without causing great damage. In d^6 ruthenium complexes the lowest energetic absorption bands in the visible region are the metal to ligand charge transfer (MLCT). Therefore, the development of new ruthenium (II) complexes with a red shift of the MLCT absorption bands is desirable for PDT. On the other hand, an improvement in the photocytotoxic activity has also been observed in ruthenium (II) complexes containing π-expansive ligands, which present long lived intraligand excited states (IL), which are sensitive to oxygen.[27,28,29]

Therefore, a compromise between the above considerations should be considered when designing new compounds that may be interesting for their application as PSs. Part of the success of a photosensitive complex lies in being able to tune their properties by modification of the electronic structures of the ligands. In this way, the energies of the frontier orbitals could be modified allowing to control their photophysical activities. In this work we have developed a family of homo- and heteroleptic polypyridyl Ru(II) complexes, **1-4** (Scheme 1), that contain 4,4'-diphenyl-2,2'-bipyridine (*dpbpy*) ligands along with 1,10-phenantroline (*phen*) or N-methyl-N'-2-pyridilimidazolium (CN-Me) (Chart 1). The carbene ligand shows a higher electron-donating character than the other polypyridyl ligands, however, *dpbpy* and *phen* display higher π delocalization.[30] These complexes have been designed in order to study their photoluminescent (PL) properties in solution and to establish a relationship between these properties and the electronic nature of the ligands in our complexes. For this purpose, photophysical properties in solution supported by TDDFT theoretical calculations have been performed. All compounds **I-IV** and **1-4** have been synthesized (Scheme 1) and characterized spectroscopically and electrochemically in solution. The crystal structures of complexes **I** and **1-3** have been analysed by X-ray diffraction. In addition, *in vitro* cellular uptake of homo- **1** and heteroleptic complexes **2-4** and the cytotoxicity of complexes **1** and **2**, both in dark and light conditions, have been assessed using a human tumorigenic cell line (SKBR-3).
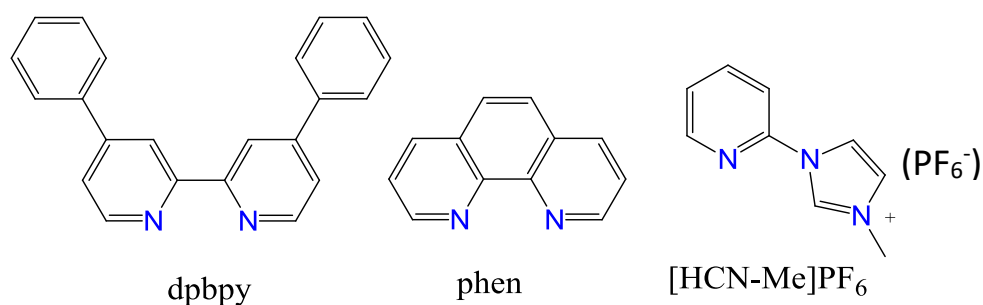
**Chart 1.** Drawing of the ligands used in this work

RESULTS AND DISCUSSION

Synthetic strategy and chemical structure

The synthetic strategy for the preparation of complexes **I-IV** and **1-4** is outlined in Scheme 1. Complexes [Ru^{II}(dpbpy)$_3$](PF$_6$)$_2$ **1**, [Ru^{II}(dpbpy)$_2$(phen)](PF$_6$)$_2$ **2**, [Ru^{II}(dpbpy)(phen)$_2$](PF$_6$)$_2$ **3** and [Ru^{II}(dpbpy)$_2$(CN-Me)](PF$_6$)$_2$ **4**, are obtained from different precursors [RuCl$_2$(dmso)$_4$],[31] *cis*-[Ru^{II}Cl$_2$(dpbpy)$_2$] **II**, *cis*-[Ru^{II}Cl$_2$(phen)$_2$] **III** and [Ru(CH$_3$CN)$_4$(CN-Me)](PF$_6$)$_2$ **IV** (Scheme 1). **II** and **III** were also synthetized by the reaction of Ru^{III}Cl$_3$·2,5 H$_2$O with the ligands *dpbpy* or *phen* in 1:2 ratio, using Zn granules (Method 1) or DMF (Method 2) as reducing agents of Ru^{III} to Ru^{II}. We have also tried to synthesize complex **II** through the reaction of [Ru^{II}Cl$_2$(DMSO)$_4$] with 2,5 mols of *dpbpy* in methanol at reflux under N$_2$ in the absence of light. In all cases, we obtained the *cis,cis*-[Ru^{II}Cl$_2$(dmso)$_2$(dpbpy)] **I,** where only one *dpbpy* ligand has been coordinated to ruthenium**.** This complex is also obtained through equimolecular amounts of [Ru^{II}Cl$_2$(dmso)$_4$] and *dpbpy* ligand in methanol. Complex **IV** was obtained from the reaction of [Ru(*p*-cymene)Cl$_2$]$_2$ and the carbene ligand in acetonitrile.

The reaction of [Ru^{II}Cl$_2$(dmso)$_4$] with 3 equiv of *dpbpy* led to the formation of complex **1** in good yield, after the addion of NH$_4$PF$_6$. Complex **2** was prepared in an easy way, through a modification of the synthesis described in the literature,[32] by reaction of **II** with *phen* in MeOH/H$_2$O. A similar procedure was used for the formation of **3** but using complex **III** as starting material and *dpbpy* ligand. Complex **4** was obtained from the reaction of **IV**, with two equiv of *dpbpy* in MeOH, leading to the substitution of the four

5

acetonitrile ligands by two *dpbpy*. Complexes **1-4** were isolated as PF_6^- salts without purification through column chromatography.
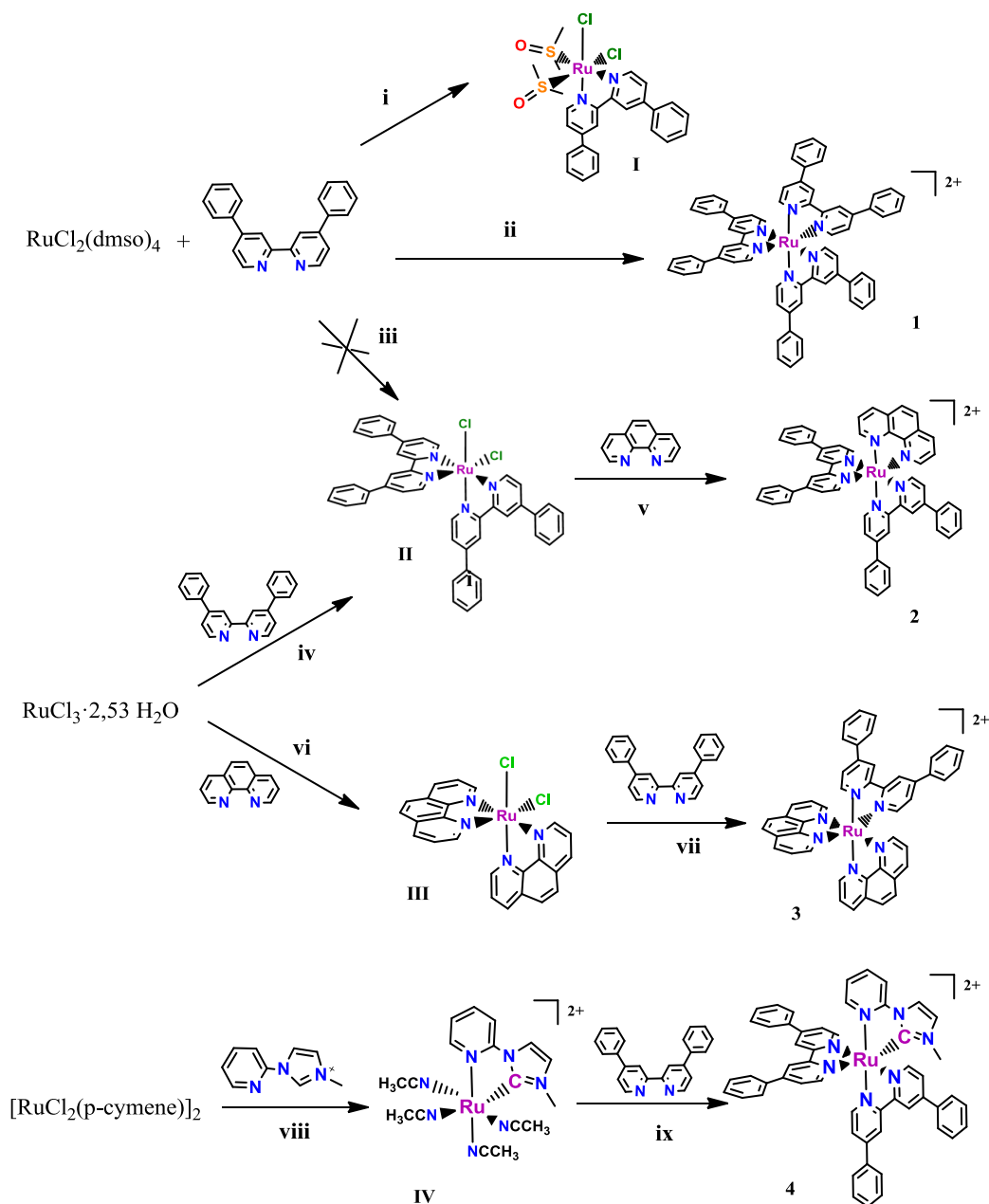
Scheme 1. Synthetic strategy for the preparation of **I-IV** and **1-4** complexes: (i) 4 h reflux in MeOH, (ii) 12 h reflux in EtOH, and precipitation with an excess of saturated aqueous solution of NH_4PF_6, (iii) 12 h reflux in MeOH using 2,5 mols of *dpbpy* (1:2,5), (iv) 12 h reflux in EtOH using LiCl and Zn granules under or 16 h reflux in DMF using LiCl, (v) 24 h reflux in MeOH/H_2O (4:1), presence of NH_4OAc and precipitation with an excess of saturated aqueous solution of NH_4PF_6, (vi) 12 h reflux in DMF using LiCl and purification in column chromatography, (v) 24 h reflux in MeOH/H_2O (4:1), NH_4OAc, precipitation with an excess of saturated aqueous solution of NH_4PF_6 and recrystallization

in CH$_2$Cl$_2$ (viii) five days heated at 45 ºC in acetonitrile in presence of KOAc and KPF$_6$, (ix) 24 h reflux in MeOH, precipitation with an excess of saturated aqueous solution of NH$_4$PF$_6$ and recrystallization in CH$_2$Cl$_2$. All synthesis was done under N$_2$ atmosphere and in the dark.

Crystal structures of **I**, **1-3** have been determined by X-ray diffraction analysis. Figures 1-2 and S1 display their molecular structures, whereas the main crystallographic data and selected bond distances and angles can be found in the Supplementary Information section (Tables S1 and S2).

In all cases, the Ru metal centres adopt a distorted octahedral type of coordination (Figure 1). In the case of complex *cis,cis*-[Ru^{II}Cl$_2$(dmso)$_2$(dpbpy)] **I**, the diphenyl-bipyridine ligand acts in a bidentate fashion through its N-atoms and the two monodentate chlorido and *dmso* ligands occupy the other four coordination positions, adopting a *cis* coordination with respect to each other. All bond distances and angles are within the expected values for this type of complexes.[33,34] It is interesting to note that the Ru-N12 bond length (2.085 Å), where the N atom is placed *trans* to the S atom of *dmso* ligand, is larger than the distance found for Ru-N23 bond (2.065 Å), where a Cl ligand is situated *trans* to the N atom. This denotes the stronger *trans* influence of the *dmso* with respect to the chlorido ligand. The complex displays two intramolecular hydrogen bonds in the equatorial plane, i) a strong hydrogen bond between the oxygen atom of the equatorial *dmso* ligand and the close hydrogen atom of the bipyridine ring (H22-O5 = 2.245 Å), then placing the methyl *dmso* groups above and below the equatorial plane; and ii) a second weak interaction takes place between the equatorial chlorido ligand and the other hydrogen atom of the bipyridine (H13-Cl3= 2.718 Å) (Figure S1a). Remarkably, the phenyl substituents are no coplanar with the bipyridine aromatic rings, showing torsion angles of 22.37 and 24.11º.

For the complexes *rac*-**1-3** all the ligands are coordinated in a bidentate fashion through their N atoms. The distorted octahedral geometries observed are due to the geometrical restrictions imposed by the *dpbpy* and *phen* bidentate ligands, presenting angles less than 90º (78.2-78.8º for *rac*-**1**, 78.13-80.78º for *rac*-**2** and 78.41-79.77º for *rac*-**3**), as a consequence other angles are larger than the 90º expected for an ideal octahedral geometry. Similar to **I** in these complexes the phenyl substituents are no coplanar with the bipyridine aromatic rings. All bond distances and angles are within the expected values for this type of complexes.[35]

7

The crystal structures of the three complexes show the presence of two enantiomers Δ and Λ as can be observed in Figures 2 and S1.

a)

b)

c)

d)
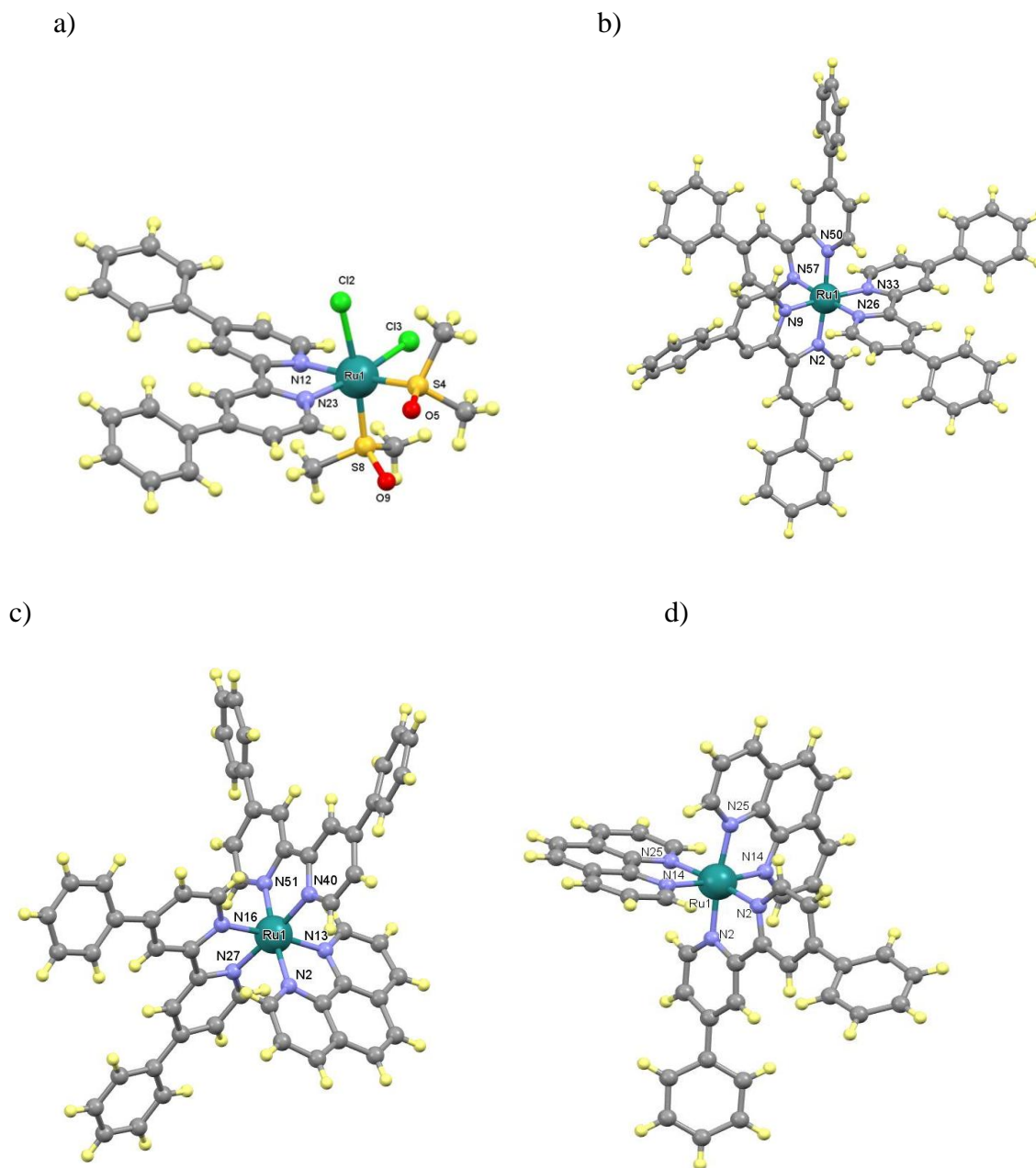
Figure 1. Crystal structures and labelling schemes for complexes **I** (a), **1** (b), **2** (c) and **3** (d).

Unlike complex *rac*-**1**, the structure of *rac*-**2** displays π-stacking interactions between the phenyl substituent of one enantiomer and one of the bipyridine rings of the other

8

enantiomer (Figure S1c). The packing of *rac*-**3** along the *b* and *c* axis shows solvent molecules and anions PF_6^- between the ruthenium cations and also π-stacking interactions between *phen* rings of neighbouring molecules (Figure S1d and S1e).
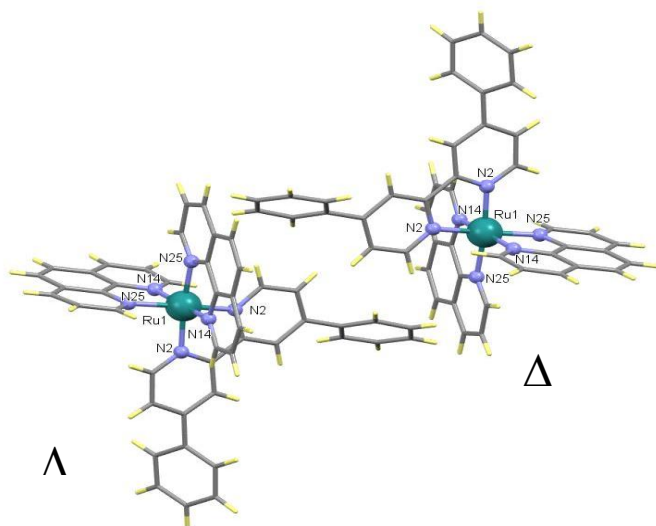
Figure 2. Crystal structures and labelling schemes for enantiomers Δ-**3** and Λ-**3.**

Spectroscopy characterization

The IR spectra of all complexes showed vibrations around 3090 cm^{-1}, which can be assigned to the ν(=C-H) stretching modes corresponding to the aromatic rings, the spectra also displayed vibrations around 1600 cm^{-1} and 1389-1412 cm^{-1}, which were assigned to ν(C=C) and ν(C=N) of the ligands. The observed peaks at 1300-1110 cm^{-1} can be assigned to δ(C-H) in the plane. In compound **I**, the vibration at around 1090 cm^{-1} was attributed to the ν(S-O) stretching due to the presence of the *dmso* ligand.

The 1D and 2D ^{1}H-NMR spectra of **I-IV** and **1-4** complexes were recorded in acetone-d$_6$, dichlorometane-d$_2$ or acetonitrile-d$_3$ and are displayed in Figures 3 and S2-S9. ^{1}H-NMR of **I** showed two sets of resonances (Figure S2), one in the aromatic region corresponding to the protons of the *dpbpy*, and four singlets in the aliphatic region, at δ = 3.50-2.57 ppm, due to the CH$_3$ of the *dmso* ligands. This pattern of resonances indicates that complex **I** is an asymmetric molecule corresponding to the *cis*(Cl), *cis*(dmso)-isomer, which is in agreement with the structure in solid state. As expected, resonances from complexes **II-III** appeared in

9

the aromatic region and can be assigned to the aromatic protons from the polypyridyl ligands *dpbpy* and *phen* (Figures S3 and S4). The spectral pattern confirms the asymmetry of the corresponding ligands when are coordinated to the Ru centre, where the two "*pyridine*" rings have different environments, which is in accordance with the presence of the *cis* isomers in both complexes. The higher deshielding observed for Hc, with respect to Hc' in **II** (10.21 vs 7.71ppm) and Ha with respect to Ha' in **III** (10.54 vs 7.84 ppm), are due to the close chlorido ligands that are placed in *cis* position to the former protons (Figure S3 and S4). For compound **IV** (Figure S5) we observed three resonances in the aliphatic region: one due to the CH_3 groups of two acetonitrile ligands in *trans* position (2.14 ppm), and two at 1.86 and 2.54 ppm corresponding to the protons of the two non-equivalent acetonitrile ligands.

The ^{1}H-NMR spectrum of the homoleptic **1** containing three bidentate *dpbpy* ligands (Figure S6) showed the same name of resonances that the spectrum of the free *dpbpy* ligand, but different chemical shifts, which indicates the symmetry of **1**. However, for the heterolytic complexes **2** and **3**, a loss of symmetry was observed by the appearance of new resonances, which indicateed different chemical environments for the protons of the two *dpbpy* or *phen* ligands in complexes **2** and **3**, respectively, due to the coordination of a different ligand (Figure 3). In both cases, the pyridinic protons (Hc and Ha) did not show high values of chemical shifts, as those observed in the starting complexes **II** and **III** (Figures S7 and S8). Both complexes **IV** and **4** revealed two set of signals (Figure S5 and S9) in the aromatic and aliphatic regions, and the disappearance of the C-H proton from the carbene ligand at 9.8 ppm clearly indicating its coordination to the metal.

It was assumed that complex **4** presents a similar geometry to **2** and **3**, however, the presence of the asymmetric carbene ligand caused a decrease of the symmetry in the molecule and the appearance of a higher number of resonances, which indicates different chemical environments for all the protons that are chemical and magnetically non-equivalent (Figure S9). The 1D- NOESY together with 2D COSY, TOCSY and NOESY NMR correlations allowed assigning most of the non-equivalent protons, however, in some cases, an overlapping of the signals is observed, especially for the different protons of the phenyl substituents, preventing the individual assignment of each of them.
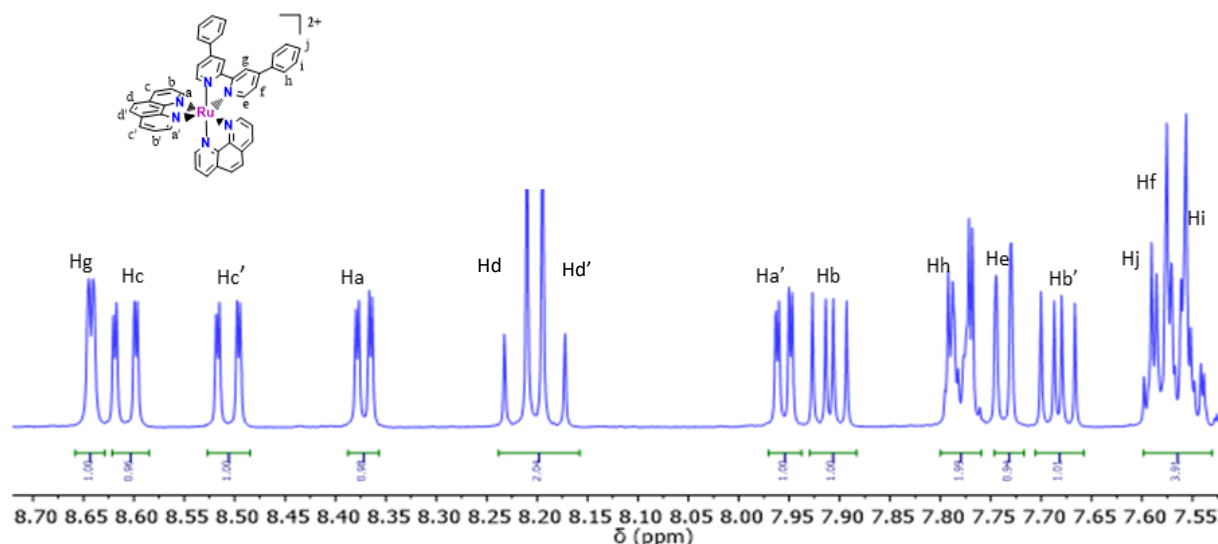
Figure 3. ^{1}H-NMR spectrum of complex **3**

The ESI-MS spectra for neutral compounds **II** and **III** displayed peaks at m/z 788.2 and 532, respectively, that can be assigned to the molecular weight of the oxidized species, $[M]^+$. For complex **IV** two peaks at m/z 528.9 and 487.9 were observed, that correspond to $[M-PF_6-CH_3CN]^+$ and $[M-PF_6-2CH_3CN]^+$ monocations, respectively. Compounds **1-4** displayed peaks corresponding to $[M-PF_6]^+$ monocations and $[M-2PF_6]^{2+}$ dications. The ESI-MS spectra are shown in Figure S10.

Photophysical Properties

The photophysical properties of the complexes have been studied by absorption and emission spectroscopy in CH_3CN and CH_2Cl_2. Tables 1 and S3 collect the photophysical data for **1-4** and the spectra are displayed in Figures 4 and S11. The UV-Vis spectra exhibited ligand based π-π^* bands below 350 nm corresponding to the polypyridyl ligands and relatively intense bands above 350 nm, mainly due to $d\pi(Ru)$-$\pi^*(L)$ MLCT transitions.[36] A different pattern of absorption bands was observed for **II** and **III** complexes, where significant absorption was observed in the visible region between 500-600 nm. These bands were attributed to $p\pi(Cl)$-$d\pi(Ru)$ LMCT transitions in related systems. [37] In contrast, investigating the charge density difference map of the corresponding transitions in **II** and **III** (Figure S12), it can be established that the transitions have $Ru(d\pi)$-π^* MLCT and $Cl(\pi)$-π^* LLCT character.

11

It is worth mentioning that all the complexes showed red shift of their MLCT transitions in comparison to the $[Ru(bpy)_3]^{2+}$ that are located at 450 nm.[27] A blue shift of 9 nm to higher energy absorptions was observed for the MLCT transitions by changing *dpbpy* to *phen* ligands in complexes **1**-**3** (Table 1 and Table S3). This agrees with the weaker σ-donor capacity of the *phen* ligand,[38] in parallel, a weaker π-acceptor character could be expected, which results in a relative stabilization of the donor dπ(Ru) orbitals caused by the *phen* ligand. In full agreement the calculated HOMO's energy level decreases in the order **1**>**2**>**3** (Figure S13-S16) *vide infra*. Moreover, complex **4** with the carbene ligand showed longer wavelength than **2** and **3** due to the higher σ-donor character, and similar values of wavelength that complex **1** with three *dpbpy* ligands. This fact may be due to the higher delocalized π electron density of the *dpbpy* ligands.

Compounds **I-IV** do not show any photoluminescent properties. A possible explanation could be the existence of non-emissive, dissociative excited states.[39,40,41] These results agreed with the DFT calculations, where ligand dissociation could be observed during the optimization of the triplet states. Since our target compounds were **1**-**4**, we have not investigated in more details these non-emissive compounds. A significant solvatochromic effect was observed for the PL properties of complexes **1-4**. The emission maxima for **1-4** was in the range from 615 to 628 nm in CH_3CN, whereas a blue shift of 4 to 15 nm was observed in the less polar CH_2Cl_2, with emission between 600 and 620 nm (Figure 4b), due to the different polarities of solvents. Compound **4** containing a CN-Me ligand featured an emission red-shift (λ_{em} = 628 nm) compare to those of **1-3**, whereas compound **3** with two *phen* ligands is blue shifted (λ_{em} = 615 nm) with regards to the other complexes. These results indicated that changing a *bpbpy* by a *phen* ligand produces a blue-shift of the emission band, whereas the introduction of a carbene ligand (CN-Me) shifts the emission to lower energies. The phosphorescence spectra of **1-4** with non vibronic structures suggest that the lowest energy excited state is mainly [3]MLCT in character. Evaluation of the phosphorescence quantum efficiency indicated that quantum yields from complexes **1-4** are nearly four times higher in CH_2Cl_2 than in CH_3CN. Complex **2** exhibited the highest phosphorescence emission with a quantum yield (Φ_P) of 44.1% in CH_2Cl_2 followed by complex **1** (Φ_P = 40%), being much lower in degassed CH_3CN (18.4% and 13.7%, respectively) under N_2 atmosphere. Contrarily, complex **4** exhibited the

lowest quantum efficiency with a Φ_P of 16%, what suggested that the introduction of the CN-Me ligand significantly decreases the emission of the parent system.

Because of the highest quantum yields measured for **1-4** in degassed CH_2Cl_2, their photophysical properties were further investigated in this solvent. On the one hand, triplet state lifetimes (τ_P) were determined under nitrogen atmosphere, which correlated with the emission quantum yields measured- i.e., higher Φ_P values were found for **1** and **2** exhibiting the largest phosphorescence efficiencies (Figure S17). On the other hand, when working with aerated CH_2Cl_2 solutions, the emission quantum yields **1-4** decreased about 3-/4-fold, as expected. However, all these complexes preserved rather large Φ_P values at this condition (> 5%), which suggested that they could be used as emission probes in biological samples. In all cases, the quantum yields dropped considerably in non-degassed solutions, which clearly evidence the effect of the O_2, indicating that the triplet emissive states are preferably consumed by non-radiative ET process via oxygen quenching. As the ^{3}MLCT state is highly sensitive to ground-state $^3O_2$, as in presence of oxygen, the energy transfer from the triplet excited state of the complex to triplet oxygen should produce the quenching of the emission intensity and possibly the generation of cytotoxic singlet oxygen ($^1O_2$), which should be favourable for PDT. To investigate the singlet oxygen photosensitizing properties of **1-4**, we used 9,10-dimethylanthracene as a specific $^1O_2$ chemical trap. DMA is well-known to undergo efficient photooxidation in the presence of $^1O_2$, which results in the disappearance of their characteristic absorption bands in the 300-400 range due to the formation of an endoperoxide product. In light of this, we investigated photometrically the photooxidation of DMA when mixed with **1-4** in CH_2Cl_2 and illuminated with visible light that is selectively absorbed by the complexes. While no intrinsic photoreactivity was observed for separate DMA under these irradiation conditions, fast DMA photobleaching was measured for the mixtures with the complexes (Figure S18). In addition, no reactivity was registered for these mixtures in the dark. Therefore, these results demonstrate the capacity of **1-4** to behave as $^1O_2$ photosensitizers. In combination with their high Φ_P, this prompted us to explore the application of these complexes *in vitro* as both emissive probes for bioimaging in confocal microscopy and PDT agents for tumorigenic mammary epithelial SKBR-3 cells (*vide infra*).

13

Table 1. Photophysical and electrochemical data of complexes **1-4**.

Complexes	λ_{abs} (nm)[a]	λ_{em} (nm)[a]	Φ_P (%)[a,b]	λ_{abs} (nm)[c]	λ_{em} (nm)[c]	Φ_P (%)[b,c]	τ_P (μs)[d]	Φ_P (%)[e]	$E_{1/2}$ (Ru^{III}/Ru^{II})(V)[f]
1	475	624	13.7	475	620	40.0	1.61	10.5	1.31
2	466	619	18.4	466	612	44.1	1.74	14.0	1.34
3	457	615	9.3	457	600	26.4	1.14	9.0	1.38
4	476	628	5.2	474	618	16.0	0.96	5.1	1.15

[a] Absorption, emission and phosphorescence quantum yields for degassed solutions in CH$_3$CN; [b][Ru(bpy)$_3$]$^{2+}$ as the standard (Φ_P = 9.4% in degassed MeCN);[42] [c] Absorption, emission and phosphorescence quantum yields for degassed solutions in CH$_2$Cl$_2$; [d]phosphorescence lifetimes measured in degassed CH$_2$Cl$_2$ solutions at λ_{exc} = 355 nm and room temperature; [e]emission quantum yields measured in air in CH$_2$Cl$_2$ solution at λ_{exc} = 445 nm, using *N,N'*-bis(butyl)-1,6,7,12-tetra-(4-*tert*-butylphenoxy)perylene-3,4:9,10-tetracarboxylic diimide as a standard (Φ_f = 1 in CH$_2$Cl$_2$)[43]; [f]CH$_2$Cl$_2$ + 0.1 M TBAH.
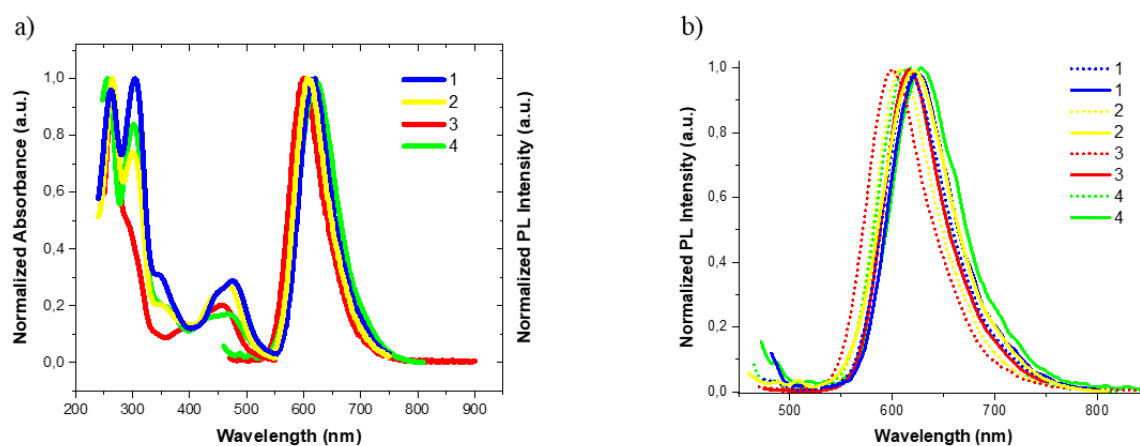
Figure 4. a) Normalized UV-visible absorption and photoluminescent (PL) emission spectra for **1-4** in CH$_2$Cl$_2$. b) Normalized emission for compounds **1-4** in CH$_3$CN (solid line) and CH$_2$Cl$_2$ (dot line).

Theoretical calculations

In order to get deeper insight into the electronic structure of these complexes, DFT calculations were performed and computed vertical transition energies were obtained using TDDFT (more details in the SI). Investigating the Kohn-Sham orbitals (Figure S13-S16 and S18-S19) in the SI), it can be established that, the central Ru has major contribution to

highest occupied molecular orbitals (HOMO-HOMO-2), while the lowest unoccupied orbitals localised at the ligands. In case of compounds **1-4**, HOMO-LUMO MLCT transition responsible for intense absorption between 457-476 nm (in acetonitrile) and as it can be expected the absorption around 300 nm belongs to ligand-centered π-π* transitions, mainly from orbitals below the energy level of HOMO-5 towards the LUMO or LUMO+1. In case of **1** and **2** the shoulder around 430-440 nm can be attributed to HOMO-2->L+1 and HOMO-1->L transitions. In case of **3** the lower level of the HOMO results blue shift of the HOMO-LUMO transitions, moreover the lower oscillator strength (which corresponds to the intensity of the peaks in the experimental spectra) were calculated of the transitions around 300 nm in full agreement with the experimental spectra. It is notable in case of **4,** the good ϭ-electron donor carbene ligand increases the energy level of the HOMO, and the double bond and the lone pairs of the nitrogen of the NHC moiety have some contribution to this orbital (Figure S16) as well.

To better identify the origin of the non-emissive character of **I-IV**, the triplet states of the above-mentioned systems were examined. It can be established that the *dmso*, CH_3CN or Cl ligands dissociate during the geometry optimization of the triplet state of **I**, **II** and **IV**, which can cause a very effective non-radiative decay. Interestingly, no ligand dissociation could be observed in complex **III** after the optimization of the triplet state. For **I** and **II** the triplet states are less stable, only 25.0 and 28.0 kcal/mol respectively (Table S17 in the SI), which means that the lack of phosphorescence can most probably be attributed to the smaller singlet-triplet gap resulting from ligand dissociation in the case of these complexes.

Electrochemical characterization

The redox properties of complexes **I-IV** and **1-4** have been studied by cyclic voltammetry (CV) experiments in CH_3CN and CH_2Cl_2 + 0.1 M TBAH, using glassy carbon (GC) as working electrodes and the redox potentials are referred to saturated calomel electrode (SCE). Table 1 and Table S18 show the summary with the redox potential values and the CV of the complexes are displayed in Figures S20 and S21. All CV exhibited one-electron oxidation wave that correspond to Ru^{III}/ Ru^{II} redox couple.

The redox potential values observed for complexes **I**, **II** and **III**, all containing two chlorido ligands, are $E_{1/2}$= 1.1, 0.37 and 0.38 V, respectively (Figure S20). The highest potential value observed for **I** is indicative of the highest π-acceptor character of two *dmso* ligands with respect to one *dpbpy* ligand in **II** and **III**. An additional wave at E_{pc}= 0.30 V is also observed in **I**, that evidences a *dmso* linkage isomerization process.[44] After oxidation of Ru^{II}(*dmso*-S) species to Ru^{III}(*dmso*-S) at E_{pa} = 1.17 V, the latter undergoes a fast linkage isomerization, forming Ru^{III}(*dmso*-O). This species is reduced to Ru^{II}(*dmso*-O) upon back-scanning, with a cathodic peak at E_{pc} = 0.30 V. The shift to lower potential values for the O-coordinated *dmso* complex is due to the lower electron-withdrawing ability of the O-coordinated *dmso*.

Voltammograms of complexes **1-4** (Figure S21) exhibited a one-electron quasi-reversible redox wave at potential values around of $E_{1/2}$ = 1.31 V (**1**), 1.34 V (**2**) 1.38 V (**3**) and 1.15 V (**4**) corresponding to the Ru^{III}/Ru^{II} redox couples. It can be observed that the trend in the redox potentials from **1** to **3** complexes becomes more positive with the increasing number of *phen* ligands in the complexes, in full agreement with the HOMO's energy level and the observed blue shift of the MLCT transitions in the absorption spectra. This evidence seems indicate that the *phen* ligand is more electron-withdrawing that the *dpbpy* ligand. On the other hand, the lowest potential value observed for complex **4**, containing the heterocycle carbene ligand, indicates that this ligand is more σ-electron donating than the polypyridilic ligands, *dpbpy* and *phen*, then doing more electron rich the ruthenium centre and easier to oxidize.

All previous results suggested that complexes **1-4** could be potential candidates as PSs for PDT, which encouraged us to accomplish preliminary biological in vitro assays to discern whether these compounds have the required properties to become PDT agents.

Biological *in vitro* studies

The complexes internalization was evaluated using confocal laser scanning microscope. Tumorigenic mammary epithelial SKBR-3 cells were incubated with 10 µg/ml of complexes **1-4** for 4 h to allow their internalization (Figure 5). Then, complexes were irradiated (light-activated) using the specific wavelength excitation light for each compound and detected according to the emission properties of the complexes. The same caption parameters were used for all complexes and results showed that SKBR-3 cells were able to internalize all of

them. Images from confocal microscopy (Figure 5) clearly showed that complexes **1** and **2** much better internalized compared to **3** and **4**. Complexes **1** and **2** demonstrated to be the most promising candidates as *in vitro* bioimaging probes due to their high luminescence emission and cellular uptake. On the contrary, complexes **3** and **4** with lower internalization and phosphorescence efficiency were not considered adequate as luminescent probes. It is well known that certain luminescent Ru (II) polypyridyl compounds containing lipophilic ligands have an affinity for hydrophobic membranes.[45,46] According to our results, we hypothesize that complex **1** with three bulky *dpbpy* ligands has the highest lipophilic character, followed by complex **2**. This would allow them to cross the cell membrane and accumulate inside the cell, whereas the introduction of *phen* or CN-Me ligands would hamper the internalization of complexes **3** and **4** in the cell.
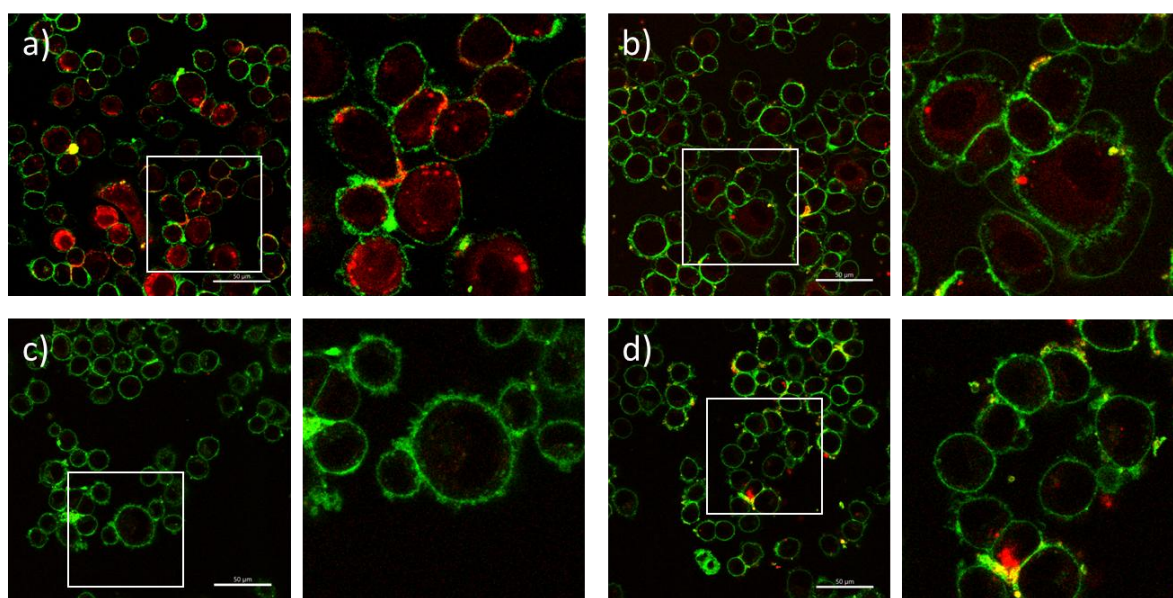
Figure 5. Confocal laser scanning microscope (CLSM) images of live SKBR-3 cells incubated with 10 µg/ml of complex **1** (a), **2** (b), **3** (c), and **4** (d) for 4 h. Cell membrane was stained by Cell Mask Deep Red Plasma Membrane dye (green) and complexes emission was detected in the red spectrum range (red). On the right of each image an enlarged area can be seen.

17

Once the internalization was verified, complexes **1** and **2** were the selected candidates to pursuit the cytotoxicity studies due to i) the degree of internalization, ii) the complex brightness and iii) the highest phosphorescence efficiency.

To evaluate the cytotoxic effect of complexes **1** and **2**, SKBR-3 cells were incubated with three different concentrations (5, 10 and 20 µg/ml) of the complex, and a control (0 µg/ml) for 4 h, and then irradiated, using an 8 W lamp and a wavelength in the range 400-600 nm for 10 min, or kept in dark conditions. The cytotoxicity of the complexes was evaluated in both light-activated and dark conditions after 48 h in culture using Alamar Blue, a metabolic activity assay.
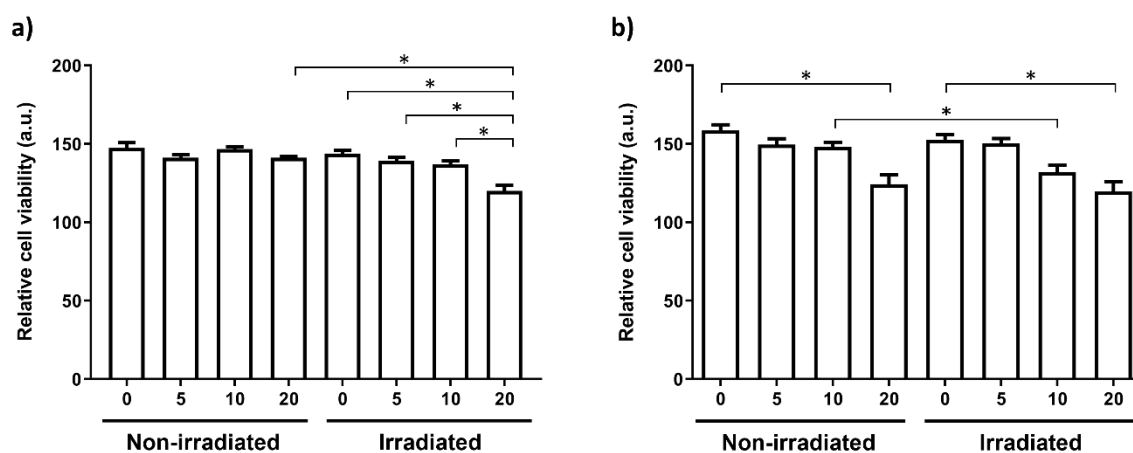
Figure 6. Cell metabolic activity for SKBR-3 cells incubated with different concentrations (5, 10 and 20 µg/ml), and a control (0 µg/ml) of complex **1** (a) and **2** (b) after 48 h post-irradiation in dark conditions (non-irradiated) and light-activated (irradiated). Asterisks denote statistical differences in the metabolic activity.

Results for complex **1** did not show cytotoxicity in dark conditions for any of the concentrations analysed (Figure 6a). However, a significant decrease in the metabolic activity was observed when cells were incubated with 20 µg/ml of complex **1** and irradiated for 10 min. The concentrations of 5 µg/ml and 10 µg/ml did not show any cytotoxic effect when irradiated.

Regarding complex **2**, results showed a significant decrease in the metabolic activity when cells were incubated with 10 µg/ml of the complex **2** and irradiated for 10 min compared to non-irradiated cells (Figure 6b). However, no significant differences were observed between irradiated and non-irradiated cells at 5 µg/ml and 20 µg/ml concentration. Regarding the effect of complex **2** on the metabolic activity in dark conditions, a significant decrease was observed when incubated with 20 µg/ml of the complex compared to control samples. In addition, no differences were observed for control samples between dark or irradiated conditions.

The metabolic activity of the cells is directly related to the cell viability, therefore these results suggested that complex **1** is not cytotoxic for any concentrations tested and **2** is cytotoxic at 20 µg/ml when incubated in dark conditions. However, when samples were irradiated, a cytotoxic effect was observed at 20 µg/ml for complex **1** and 10 µg/ml for complex **2**. These results indicated that light-activated complexes **1** and **2** were able to induce cell death on tumorigenic mammary epithelial SKBR-3 cells without any deleterious effect when in dark conditions. We hypothesize that these two complexes generate ROS which lead to intracellular damage and cell death.[21,25] Thus, the results obtained for internalization and cytotoxicity analyses denoted the potential of both complexes as a candidate for PDT.

The results indicate that complex **1** would be a good candidate for PDT as it presents a balance between its hydrophobic character and its cytotoxic properties.[47] On the one hand, its hydrophobicity seems suitable for cellular uptake and intracellular accumulation, particularly within the cytoplasm. Remarkably, even at a concentration as high as 20 µg/ml, complex **1** exhibits negligible cytotoxicity in the absence of light activation. In contrast, complex **2**, while similarly proficient in cellular internalization, manifests a degree of cytotoxicity prior to light activation at the same concentration of 20 µg/ml.

CONCLUSIONS

A series of homo- (**1**) and heteroleptic Ru(II) polypyridyl complexes (**2-4**), containing 4,4'-diphenyl-2,2'-bipyridine (*dpbpy*) and 1,10-phenantroline (*phen*) or N-methyl-N'-2-pyridilimidazolium (*CN-Me*) ligands, have been successfully synthesized and studied as potential PDT photosensitizers. Their structures in solid and solution were fully confirmed by

X-ray diffraction, multinuclear NMR and ESI-MS measurements. For all complexes, the UV-Vis spectra displayed ligand based π-π* bands at high energies corresponding to the polypyridyl ligands and relatively intense MLCT transitions in the range 457-476 nm, that were red shifted when changing *phen* by *dpbpy* or CN-Me ligands, due to the weaker σ-donor capacity of *phen*. A different pattern of absorption bands was observed for the starting chlorido complexes, corresponding to pπ(Cl)-dπ(Ru) LMCT transitions, in the visible region between 500-600 nm. DFT calculations confirmed that the HOMO-LUMO MLCT transition is responsible for the intense absorptions between 457-476 nm and the absorption around 300 nm belongs to ligand-centered π-π* transitions, mainly from orbitals below the energy level of HOMO-5 towards the LUMO or LUMO+1. The electrochemical studies showed one-electron oxidation waves corresponding to Ru^{III}/ Ru^{II} redox couple, with the exception of complex **I** where an additional wave at E_{pc}= 0.30 V is also observed, that evidences a *dmso* linkage isomerization process. For **1-4** the redox potentials become more positive when increasing the number of *phen* ligands in the complexes, in full agreement with the energy level of the HOMO and the observed blue shift of the MLCT transitions in the absorption spectra.

Starting **II-IV** did not show any PL properties, whereas their derivatives **1-4** displayed phosphorescence emission in the range from 615 to 628 nm in CH_3CN and in the range from 600 to 620 nm in CH_2Cl_2, indicating a solvatochromic effect. Studies using degassing solutions confirmed the triplet nature of the emissive states (^{3}MLCT). In both solvent, complexes **1** and **2** exhibited the highest phosphorescence emission with quantum efficiencies of 40.0% and 44.1% in degassed CH_2Cl_2, respectively. On the contrary, complex **4** showed low quantum efficiency suggesting that the introduction of a carbene ligand produces a significant quenching of the phosphorescence. All of them show lower quantum yields in aerated solutions Furthermore, complexes **1-4** have phosphorescence triplet state lifetime in the range 0.96 and 1.74 μs in degassed CH_2Cl_2. TDDFT theoretical analysis seems to indicate that the origin of the non-emissive character of **I**, **II** and **IV** is the dissociation of *dmso*, CH_3CN or Cl ligands.

Complexes **1** and **2** displayed the highest luminescence efficiency and cellular uptake in tumorigenic mammary epithelial SKBR-3 cells and demonstrated to induce cell death after

light-activation. However, an important difference between the two complexes must be stressed: while complex **2** shows a certain cytotoxicity in dark conditions, which rules it out as a PDT agent, complex **1** seems to possess a perfect balance between its hydrophobicity and low cytotoxic properties in the dark. These results suggest that complex **1** could be a good candidate as theranostic agent for bioimaging and PDT.

The development of these type of complexes allows for the construction of future light-activated molecules which are able to act as highly reactive PDT agents that can be excited with red light and use oxygen-independent mechanisms of action. We will continue to strive and work on the development of synthetic methodologies and improved purification methods for the production of new systems based on polypyridyl Ru complexes, as well as the study of their photophysical properties and biomedical applications.

EXPERIMENTAL SECTION

Materials

All reagents used in the present work were obtained from Sigma-Aldrich and were used without further purification. Reagent grade organic solvents were obtained from Carlo Erba and high purity de-ionized water was obtained by passing distilled water through a nano-pure Mili-Q water purification system. 3-methyl-1-(pyridin-2-yl)-1*H*-imidazol-3-ium hexafluorophosphate (HCN-Me)PF$_6$ ligand was prepared according to literature procedures.[48]

Instrumentation and Measurements

IR spectra were recorded on an Agilent Cary 630 FTIR spectrometer equipped with an ATR MK-II Golden Gate Single Reflection system. Cyclic voltammetry (CV) and Differential Pulse Voltammetry (DPV) experiments were performed in an IJ-Cambria 660C potentiostat using a three electrode cell. Glassy carbon electrode (3 mm diameter) from BAS was used as working electrode, platinum wire as auxiliary and SCE as the reference electrode. The complexes were dissolved in solvents containing the necessary amount of n-Bu$_4$N$^+$PF$_6^-$ (TBAH) as supporting electrolyte to yield a 0.1 M ionic strength solution. All $E_{1/2}$ values reported in this work were estimated from cyclic voltammetry experiments as the average of

the oxidative and reductive peak potentials $(E_{pa}+E_{pc})/2$. The NMR spectroscopy was performed on Bruker DPX 300 and 400 MHz spectrometers. Samples were run in CD_2Cl_2, CD_6CO or CD_3CN. Elemental analyses were performed using a CHNS-O Elemental Analyser EA-1108 from Fisons. ESI-MS experiments were performed on a Navigator LC/MS chromatograph from Thermo Quest Finnigan, using acetonitrile as mobile phase.

Crystallographic Data Collection and Structure Determination

The X-ray intensity data were measured on a Bruker D8 QUEST ECO three-circle diffractometer system equipped with a Ceramic x-ray tube (Mo Kα, λ = 0.71076 Å) and a doubly curved silicon crystal Bruker Triumph monochromator, using APEX3 software package.[49]The frames were integrated with the Bruker SAINT.[50] Data were corrected for absorption effects using the Multi-Scan method (SADABS).[51] The structures were solved and refined using the Bruker SHELXTL.[52]

The crystallographic data as well as details of the structure solution and refinement procedures are reported in supplementary information. CCDC 2235126 (for *cis,cis*-**I**), 2235127 (for **1**), 2235128 (for **2**), and 2235125 (for **3**) contain the supplementary crystallographic data for this paper.

Synthesis and characterization of the complexes

Synthesis of *cis,cis*-[RuCl$_2$(dpbpy)(dmso)$_2$], I. A mixture of dpbpy ligand (0.1 g, 0.32 mmol) and [RuCl$_2$(dmso)$_4$] (0.124g, 0.27 mmol) were dissolved in 15 ml de methanol and the resulting solution refluxed for 4h, under N$_2$ atmosphere and in the dark. An orange-brown solid was formed and was filtered on a frit, washed with ether and vacuum-dried. Yield:137 mg (75%). Anal. Found (Calc.) for C$_{26}$H$_{28}$N$_2$Cl$_2$O$_2$S$_2$Ru: C, 47.37 (47.41); H, 4.12 (4.68); N, 4.79 (4.40). IR (ν, cm^{-1}): 3063, 2925, 1610, 1539, 1472, 1409, 1297, 1308, 1233, 1099, 1088, 1017, 1002, 958, 898, 864, 868, 775, 760, 734, 715, 686. ^{1}H-RMN (400 MHz, CD$_2$Cl$_2$): δ 9.80(d, J=5.92Hz, 1H, H$_c$), 9.74(d, J=6.08Hz, 1H, H$_{c'}$), 8.48(d, J=1.68Hz, 1H, H$_a$), 8.44(d, J=2.0Hz, H$_{a'}$), 7.80(m,5H, H$_b$, H$_d$, H$_{d'}$), 7.68(dd, J=6.08Hz, J=2.04Hz, 1H, H$_{b'}$), 7.60 (m,6H,

H_f, $H_{f'}$, H_e, $H_{e'}$), 3.50(s,3H), 3.49 (s,3H) 3.15 (3H), 2.57 (3H). ^{13}C-NMR (400 MHz, CD_2Cl_2): δ 156 ($C_{c'}$), 152 (C_c), 120.5 ($C_{a'}$), 120 (C_a), 127(C_b, C_d, $C_{d'}$), 123 ($C_{b'}$), 130 (C_f, $C_{f'}$, C_e, $C_{e'}$), 46, 45, 44 (C_{CH3}). UV-Vis (CH_2Cl_2) [λ_{max}, nm (ε, M^{-1} cm^{-1})]: 260 (213334), 299 (186667), 399 (31000). $E_{1/2}$ (CH_2Cl_2 + 0.1M TBAH) = 1.1 V V vs. SCE.

Suitable crystals of *cis-cis*-**I** were grown as pale-yellow plates by diffusion of diethyl ether into a CH_2Cl_2 solution of the solid.

Synthesis of *cis*-[RuCl$_2$(dpbpy)$_2$], II. *Method 1.* A mixture of $RuCl_3 \cdot 2,53$ H_2O (0.205 g, 0.81 mmol), dpbpy (0.5 g, 1.62 mmol), LiCl (0.1g, 2.43 mmol) and Zn granules (0.16 g, 2.43 mmol) was heated at reflux in 50 ml of EtOH for 12 h, under N_2 atmosphere and in the dark. The reaction mixture was filtered, and a purple-black solid was obtained. Yield: 630 mg (94%). *Method 2.* A mixture of $RuCl_3 \cdot 2,53$ H_2O (0.150g, 0.593mmol) and DMF (5ml) was stirred under nitrogen for 5 minutes, then LiCl (0.162g, 3.809 mmol) is added to the mixture and stirred until its total dissolution. Then dpbpy (0.366g, 1.186 mmol) along with DMF (5ml) was added. The mixture refluxed under N_2 atmosphere for 16 h to give a black solution. The solution was left to cool at room temperature, then acetone (30 ml) was added and the solution was cooled in the freezer overnight. The obtained product was filtered, washed with ether and vacuum dried. Yield: 364.7 mg (78%).

Anal. Found (Calc.) for $C_{44}H_{32}N_4Cl_2Ru$: C, 66.8 (67.0); H, 4.50 (4.09); N, 7.11 (7.10).

IR (ν, cm^{-1}): 3067, 3063, 1610, 1535, 1464, 1409, 1360, 1248, 1014, 909, 846, 760, 734, 689. ^{1}H-RMN (400MHz, CD_2Cl_2): δ 10.21 (d, J=5.9Hz, 2H, H_c), 8.61(s, 2H, H_a), 8,44(s, 2H, $H_{a'}$) , 7.94 (d, J= 7.5Hz, 4H, H_d) , 7.83 (d, J=5.8Hz, 2H, H_b), 7.71(d, J=6.1Hz, 2H,$H_{c'}$), 7.69-7.59(m, 8H, H_e,$H_{e'}$), 7.55(t, J=7.3Hz, 2H, H_f) , 7.46 (dq, J=14.0, 7.0Hz, 6H, $H_{d'}$,$H_{f'}$), 7.14(d, J=5.9Hz, 2H, $H_{b'}$). ^{13}C NMR (400MHz, CD_2Cl_2): δ 160 (C_q); 158 (C_q); 154.8, (C_c); 152.5 (C_b); 146.7 (C_q); 145.5 (C_q); 137.3 (C_q); 136.4 (C_q); 129.6, (C_e); 129.5 ($C_{e'}$); 129.3 (C_f); 129.2 ($C_{f'}$); 127.2 (C_d); 126.9 ($C_{c'}$); 123.6 (C_d); 122.8 ($C_{b'}$); 120.6 ($C_{a'}$); 119.7 (C_a). UV/Vis (CH_2Cl_2), [λ_{max} nm (ε, cm^{-1} M^{-1})]: 256 (51860), 381 (11273). $E_{1/2}$(Ru^{III}/Ru^{II})(CH_2Cl_2 + 0.1M TBAH): 0.371 V vs SCE. ESI-MS [*m/z*]: 788.2 [M^+].

Synthesis of *cis*-[RuCl$_2$(phen)$_2$], III.   A mixture of RuCl$_3$·2,53 H$_2$O (0.20g, 0.79mmol), phen (0.285 g, 1.581 mmol) and LiCl (0.23 g, 5.53 mmol) was heated at reflux and stirred in 20 ml of DMF for 12 h, under N$_2$ atmosphere and in the dark. The solution was left to cool at room temperature, then a black solid was precipitated. The obtained product was filtered and purified in column chromatography (Al$_2$O$_3$, eluent CH$_2$Cl$_2$/MeOH, 99/1). Yield: 141 mg (33.5%).

IR (ν, cm^{-1}): 3040, 1565, 1423, 1404, 1281, 1192, 1091, 1047, 838, 719. ^{1}H-RMN (400MHz, CD$_2$Cl$_2$): δ 10.54 (dd, J$_{a-b}$=5.3Hz, J$_{a-c}$=1.3Hz, 2H, H$_a$), 8.47 (dd, J$_{c-b}$=8.2Hz, J$_{c-a}$=1.3Hz, 2H, H$_c$), 8.11 (d, J$_{d-d}$=8.8Hz, 2H, H$_d$), 8.08 (dd, J$_{b-c}$=8.2Hz, J$_{b-a}$=5.3Hz, 2H, H$_b$), 8.01 (dd, J$_{c'-b'}$=8.1Hz, J$_{c'-a'}$=1.2Hz, 2H, H$_{c'}$), 7.96 (d, J$_{d'-d}$=8.8Hz, 2H, H$_{d'}$), 7.84 (dd, J$_{a'-b'}$=5.4Hz, J$_{a'-c'}$=1.2Hz, 2H, H$_{a'}$), 7.20 (dd, J$_{b'-c'}$=8.1Hz, J$_{b'-a'}$=5.4Hz, 2H, H$_b$). ^{13}C NMR (400MHz, CD$_2$Cl$_2$): δ 154.65 (C$_a$), 152.8 (C$_{a'}$) 133.33 (C$_c$), 131.55 (C$_{c'}$), 127.34 (C$_{d'}$), 127.25 (C$_d$), 125.1 (C$_b$), 123.61 (C$_{b'}$). UV/Vis CH$_2$Cl$_2$), [λ$_{max}$ nm (ε, cm^{-1} M^{-1})]: 267(67500), 550(12300). E$_{1/2}$(Ru^{III}/Ru^{II})(CH$_2$Cl$_2$ + 0.1M TBAH): 0.38 V vs SCE. ESI-MS [*m/z*]: 532 [M$^+$].

Synthesis of [Ru(CH$_3$CN)$_4$(CN-Me)](PF$_6$)$_2$, IV.   A mixture of [Ru(p-cymene)Cl$_2$]$_2$ (0.1g, 0.163 mmol), (CN-Me)PF$_6$ (0.099g, 0.326 mmol), KOAc (0.064g, 0.652 mmol) and KPF$_6$ (0.12g 0.652 mmol) was heated at 45 ºC in 20 ml of acetonitrile and stirred for five days, under N$_2$ atmosphere and in the dark. Afterwards, the resulting solution was filtered and the solution was removed. After the addition of diethyl ether was obtained a light brown solid, which was filtered and dried. Yield: 211 mg (90.5%).

IR (ν, cm^{-1}): 3300, 1494.27, 14043.83,823.52. ^{1}H-RMN (400MHz, CD$_3$CN): δ 8.87 (d, 1H, H$_1$), 8.15 (t, 1H, H$_2$), 8.0 (d, 1H, H$_5$), 7.83 (d, 1H, H$_4$), 7.44 (t, 1H, H$_3$), 7.38 (d, 1H, H$_6$), 4.05 (s, 3H, H$_7$), 2,54(s, 3H, CH$_3$CN), 2,14(s, 6H, CH$_3$CN), 1.86 (s, 3H, CH$_3$CN). ^{13}C NMR(400MHz, CD$_2$Cl$_2$): δ 152(C$_1$), 140.8(C$_2$), 125.3(C$_6$), 122(C$_3$), 116.6(C$_5$), 111.3(C$_4$), 36.8(C$_{CH3}$), 21.4(C$_{CH3CN}$), 3.55(C$_{CH3CN}$), 3.1(C$_{CH3CN}$). UV/Vis (CH$_3$CN), [λ$_{max}$ nm (ε, cm^{-1} M^{-1})]: 600(9843),338(62148), 265.5(246857). E$_{pa}$(Ru^{III}/Ru^{II})(CH$_3$CN+ 0.1M TBAH): 1.17 V vs SCE. ESI-MS [*m/z*]:528.9, [M-PF$_6$-CH$_3$CN]$^+$; 487,9 [M-PF$_6$-2CH$_3$CN].$^+$

Synthesis of [Ru(dpbpy)₃](PF₆)₂ , 1. A mixture of $Ru^{II}Cl_2(dmso)_4$ (0.1g, 0.22 mmol) and dpbpy ligand (0.26g, 0.87mmol) en 15 ml of EtOH was heated at reflux for 12 h, under N_2 atmosphere and in the dark. Afterwards, the solution was left to cool at room temperature, then after addition of a saturated aqueous solution of NH_4PF_6 a red-orange precipitate was formed which was filtered off and washed with cold water and ether and vacuum dried. Yield: 240 mg (83%). Anal. Found (Calc.) for $C_{66}H_{48}N_6RuP_2F_{12}$: C, 60.39 (60.23); H, 3.35 (3.68); N, 6.48 (6.39). IR (ν, cm^{-1}): 3055, 1609, 1468, 1408, 827, 760, 693. ^{1}H-RMN (400MHz, $(CD_3)_2CO$): δ 9.40 (s, 1H, H_a), 8.30 (d, J=6.0Hz, 1H, H_c), 7.99 (dd, J=7.9, 1.6Hz, 2H, H_d), 7.94 (dd, J= 6.0, 1.9Hz, 1H, H_b), 7.64-7.53 (m, 3H, H_e,H_f). ^{13}C NMR (400MHz, $(CD_3)_2CO$): δ 158.8 (C_i), 152.84(C_b), 150.59(C_g), 136.68(C_h), 131.41(C_f), 130.35(C_e), 128.33(C_d), 126.07(C_c), 123.03(C_a). UV/Vis (CH_2Cl_2), [λ_{max} nm (ε, cm^{-1} M^{-1})]: 262 (109000), 348 (32270), 475 (28950). $E_{1/2}(Ru^{III}/Ru^{II})(CH_2Cl_2$ + 0.1M TBAH): 1.31 V vs SCE. ESI-MS [m/z]: 1171.2 [M-PF₆]$^+$; 513.2 [M-2PF₆].$^{2+}$

Synthesis of [Ru(dpbpy)₂(phen)](PF₆)₂, 2. The complex was synthetized following a different method described in the literature.[32] A mixture of **II** (0.043g, 0.054mmol), ligand 1,10-fenantrolina, phen (0.011g, 0.060mmol) and NH_4OAc (0.009g, 0.11mmol) was refluxed in 30ml of MeOH/H₂O (4:1) during 24 h, under N_2 atmosphere and in the dark. Afterwards, the solution was left to cool at room temperature, then after addition of a saturated aqueous solution of NH_4PF_6 an orange precipitate was formed. The solid was filtered off and washed with cold water and diethylether and vacuum dried. Yield: 45,5 mg (67%). Anal. Found (Calc.) for $C_{56}H_{40}N_6RuP_2F_{12}\cdot2H_2O$: 54.74 (54.95); H, 3.18 (3.62); N, 6.91 (6.87). IR (ν, cm^{-1}): 3051,1609, 1468, 1408, 819, 760. ^{1}H-RMN (400MHz, (CD_2Cl_2)): δ 8.68 (s, 2H, H_a), 8.64 (s, 2H, $H_{a'}$), 8.59 (d, J=8.1 Hz, 2H, H_1), 8.30 (d, J=4.6 Hz, 2H, H_c), 8.22 (s, 2H, H_4), 8.05(d, J=5.9Hz , 2H, $H_{c'}$), 7.92(d, J=6.7Hz, 2H, H_2), 7.897.85 (m, 3H, $H_{b,}$ H_f), b'7.80-7.74(m, 6H, $H_e,H_{b'}$), 7.63(d, J=5.9Hz, 2H, H_3), 7.61(s, 4H, $H_{d'}$), 7.-7.51(m, 14H, H_e, $H_{e'}$, H_d, H_f). ^{13}C NMR(400MHz, $(CD_3)_2CO$): δ 152(C_c), 151.7($C_{c'}$), 136 (C_1), 130-125 (C_d, C $_{d'}$, $C_{e'}$, C_f)127,9 (C_4), 127.4(C_2), 127(C_3), 126.8(C_b, C_f), 125-127 ($C_{b'}$, C_e) 121.33($C_{a'}$), 121.3(C_a). UV/Vis (CH_2Cl_2), [λ_{max} nm (ε, cm^{-1} M^{-1})]: 265 (120000), 297 (78000), 466 (24400).

$E_{1/2}(Ru^{III}/Ru^{II})(CH_2Cl_2 + 0.1M$ TBAH): 1.34 V vs SCE. ESI-MS [m/z]: 1043.2 [M-PF$_6$]$^+$, 449.1 [M-2PF$_6$]$^{2+}$.

Synthesis of [Ru(phen)$_2$(dpbpy)](PF$_6$)$_2$, 3. A mixture of **III** (0.084g, 0.158 mmol), lligand dpbpy (0.0487g, 0.158 mmol) and NaOAc (0.0388g, 0.474 mmol) was refluxed in 50 ml of MeOH/H$_2$O (4:1) during 24 h, under N$_2$ atmosphere and in the dark. Afterwards, the solution was left to cool at room temperature, then after addition of a saturated aqueous solution of NH$_4$PF$_6$ a orange-red precipitate was formed. The solid was filtered and recrystallized in CH$_2$Cl$_2$. Yield: 111 mg (66.43% %). Anal. Found (Calc.) for C$_{46}$H$_{32}$N$_6$RuP$_2$F$_{12}$: 52.42 (52.13); H, 3.18 (3.04); N, 7.74 (7.93). IR (ν, cm^{-1}): 2917, 1613, 1423, 1103, 827, 764, 719, 700. ^{1}H-RMN (400MHz, (CD$_2$Cl$_2$): δ 8.64 (dd, J$_{g-h}$=2.1Hz, J$_{g-f}$=0.6Hz, 2H, H$_g$), 8.61 (dd, J$_{c-b}$=8.3Hz, J$_{a-c}$=1.2Hz, 2H, H$_c$), 8.51 (dd, J$_{c'-b'}$= 8.3Hz, J$_{a'-c'}$=1.3Hz, 2H, H$_{c'}$), 8.37 (dd, J$_{a-b}$=5.3Hz, J$_{c-a}$=1.2Hz, 2H, H$_a$), 8.22 (d, J$_{d-d'}$=8Hz, 2H, H$_d$), 8.18 (d, J$_{d'-d}$=8Hz, 2H, H$_{d'}$), 7.96 (dd, J$_{a'-b'}$=5.3Hz, J$_{c'-a'}$=1.3Hz, 2H, H$_{a'}$), 7.91 (dd, J$_{b-c}$=8.3Hz, J$_{b-a}$=5.3Hz, 2H, H$_b$), 7.74 (d, J$_{e-f}$=6Hz, 2H, H$_e$), 7.68 (dd, J$_{b'-c'}$=8.3Hz, J$_{b'-a'}$=5.3Hz, 2H, H$_{b'}$), 7.59 (d, J$_{j-i}$=2Hz, 2H, H$_j$), 7.58-7.55 (m, 4H, 2H$_f$, 2H$_i$). ^{13}C NMR(400MHz, (CD$_2$Cl$_2$): δ 153.27(C$_a$), 152.90(C$_{a'}$), 152.55(C$_e$), 137.52(C$_c$), 137.38(C$_{c'}$), 130.15(C$_i$), 128.84(C$_d$), 128.79(C$_{d'}$), 127.85(C$_h$), 127.12(C$_b$) 126.99(C$_{b'}$), 126.28(C$_f$), 125(C$_j$) 122.09(C$_g$). UV/Vis (CH$_2$Cl$_2$), [λ$_{max}$ nm (ε, cm^{-1} M^{-1})]: 264(145000), 382(16600), 456 (23600). $E_{1/2}(Ru^{III}/Ru^{II}$)(CH$_2$Cl$_2$ + 0.1M TBAH): 1.38 V vs SCE. ESI-MS [m/z]: 915, [M-PF$_6$]$^+$; 385, [M-2PF$_6$]$^{2+}$.

Synthesis of [Ru(dpbpy)$_2$(CN-Me)](PF$_6$)$_2$, 4. A mixture of **IV**(0.05g, 0.07 mmol), *dpbpy* (0.043g, 0.14 mmol) was refluxed in 20 ml of MeOH during 24 h, under N$_2$ atmosphere and in the dark. Afterwards, the solution was left to cool at room temperature, then after addition of a saturated aqueous solution of NH$_4$PF$_6$ a brown-orange precipitate was formed. The solid was filtered and recrystallized in CH$_2$Cl$_2$. Yield: 29 mg (35.74 %). Anal. Found (Calc.) for C$_{52}$H$_{41}$N$_7$RuP$_2$F$_{12}$: 54.30 (54.08); H, 3.23 (3.58); N, 8.17 (8.49). IR (ν, cm^{-1}): 1584, 1539, 1453, 1360, 1036, 831, 756, 682.^{1}H-RMN (400MHz, (CD$_2$Cl$_2$): δ 8.64, 8.61, 8.60, 8.58 (s, 4H, H$_{a,a',a'',a'''}$), 8.06 (d, 1H, H$_{c,}$), 8.03(d, 1H, H$_1$), 7.98(d, 1H, H$_5$), 7.96(d, 1H, H$_{c'}$), 7.814(d, 1H, H$_{c''}$), 7.70(1H, H$_{c'''}$), 7.9-7.7(m, 8H, H$_d$), 7.68(1H, H$_3$), 7.63(d, 1H, H$_b$), 7.54(1H, H$_4$),

7.6-7.5(m, 3H, $H_{b', b'', b'''}$, 8 H, $_{e,f}$), 7.4-7.3(m, 4H, H_e, H_f,), 7.28(m, 1H, H_2), 7.26(d, 1H, H_6), 3.26(s, 3H, H_7). UV/Vis (CH_2Cl_2), [λ_{max} nm (ε, cm^{-1} M^{-1})]: 474(12000), 296(63560), 254(96800). $E_{1/2}(Ru^{III}/Ru^{II})$($CH_2Cl_2$ + 0.1M TBAH): 1.15 V vs SCE. ESI-MS [m/z]: 1022, $[M-PF_6]^+$; 438.7 $[M-(2PF_6)]^{2+}$.

Photophysical measurements

Optical properties were evaluated in anhydrous grade CH_3CN and CH_2Cl_2 purchased from Sigma Aldrich and used without further purification. UV-vis absorption spectra were recorded on a JASCO V-780 UV-Visible/NIR spectrophotometer using 1-cm path length cuvettes. For each compound, measurements were conducted at different concentrations within the range 10^{-4} to 10^{-5} M to calculate their molar extinction coefficients (ε). Phosphorescence emission spectra were measured using two different spectrometers: (a) a VARIANT Cary Eclipse spectrometer, with which phosphorescence excitation spectra were also recorded (excitation and emission slits = 2.5 mm); (b) a custom-made emission spectrometer, where emitted photons are detected in an Andor ICCD camera coupled to a spectrograph that allows conducting time-resolved spectral measurements. Appropriate excitation wavelengths were selected in each case to maximize phosphorescence emission while preventing overlap with scattering photons. Fluorescent contaminants were not detected on excitation at the wavelength region of experimental interest for any of the samples, while sample concentration was adjusted to have an absorbance between 0.1 and 1 at λ_{exc} to avoid inner filter effects. All the emission measurements were carried out in 1-cm four-sided quartz cuvettes from Hellma Analitics and samples were previously degassed with a nitrogen flow to avoid triplet state quenching by molecular oxygen.

Phosphorescence quantum yields (φ) were determined using equation (1) and an external standard: $[Ru(bpy)_3]^{2+}$ (Φ_P = 9.4% in degassed MeCN)[42] or N,N'-bis(butyl)-1,6,7,12-tetra-(4-*tert*-butylphenoxy)perylene-3,4:9,10-tetracarboxylic diimide (Φ_f = 1 in CH_2Cl_2).[43]

$$\phi = \phi_{STD} \frac{I}{I_{STD}} \frac{Abs_{STD}}{Abs} \frac{n^2}{n_{STD}^2} \qquad (1)$$

In equation 1 ϕ_{STD} is the phosphorescence quantum yield of the standard, I and I_{STD} are the integrated area of the emission band of the sample and the standard, respectively, Abs and Abs_{STD} are the absorbance at the excitation wavelength for the sample and the standard,

respectively, and n and n_{STD} are the solvent refractive index of the sample and the standard solutions, respectively.

Phosphorescence lifetimes were measured with our custom-made spectrometer using the third harmonic of a Nd:YAG laser (Brilliant, λexc = 355 nm, pulse width = 6 ns) as excitation source. Time-resolved spectra were collected with a time resolution of 50 ns from 0 to 10 μs, and the time decay of the integrated emission intensity was fitted with a monoexponential function to obtain the characteristic τ_P value.

9,10-dimethylanthracene (DMA) was used as chemical trap to investigate the singlet oxygen photosensitizing properties of complexes **1**-**4**. With this aim, mixtures of DMA and complexes **1**-**4** were prepared in CH_2Cl_2 (c_{DMA} = 14.0 10^{-5} M, c_{1-4} = 2.0 10^{-5} M) and the variation of their absorption spectra upon visible light irradiation was measured in time. In these experiments, selective irradiation of the complexes was accomplished by using a 435LP long-pass filter to spectrally remove the violet component of a white light LED source (power = 28 mW cm^{-2}). Control experiments were also conducted to investigate the photostability of DMA under equivalent illumination conditions as well as the stability of the mixtures of DMA and complexes **1**-**4** in the dark.

Theoretical calculations

The Gaussian 16 program package[53] was used for all calculations, while Molden 4.3[54] and IQmol 2.15.0[55] were used for the visualization of the computed structures and orbitals. For visualization of the TD-DFT results Gaussum program was used.[56]

The investigated systems were optimized at the B3LYP/6-31G* (LANL2DZ for Ru) level of theory. This level of theory was succesfully applied for similar systems.[4] TD-DFT calculations were carried out at several theoretical levels (Table S3-S8) for example CAM-B3LYP/6-31G* (LANL2DZ for Ru), which showed a blue shift compared to the experimental results. The utilization of PBE1PBE/6-31G* (LANL2DZ for Ru) resulted in a strong red shift for compounds **I** and **II**. The B3LYP/6-31G* (LANL2DZ for Ru) with an acetonitrile solvent model provided well-correlating data with the experimental results for molecules **1**-**4**, however, even though LANL2DZ has been used in previous literature for

molecules containing Ru, some TD-DFT calculations were made at the B3LYP/def2-TZVP level of theory. This resulted in a small red shift, which might better describe (slightly) the UV-VIS spectra of **1-4**.

Cell culture

Human tumorigenic mammary epithelial SKBR-3 cells (ATCC, USA) were cultured in McCoy's 5A modified medium (ThermoFisher Scientific, USA) supplemented with 10% foetal bovine serum (ThermoFisher Scientific, USA) under standard conditions (37°C and 5% CO_2). For internalization of the complexes, 200,000 cells were seeded in special glass bottom confocal 35 mm dishes (Ibidi, DE) and cultured for 24 h. For the cytotoxicity of the complexes both in dark and light-activated samples, 50,000 cells were seeded in 24 well-plates and cultured for 24 h to allow cell adhesion.

Internalization of the complexes

The *in vitro* internalization of complexes **1-4** into SKBR-3 cells was evaluated under confocal laser scanning microscope. The complexes were diluted in DMSO (Sigma) to a concentration of 2 mg/ml, and then diluted in McCoy's 5A modified medium to obtain a final concentration of 10 µg/ml. After 24 h of cells growing in standard conditions, cells were incubated with 10 µg/ml of each complex for 4 h. Then, cells were washed with saline solution and fresh medium was added. Cells were stained with Cell Mask Deep Red Plasma Membrane dye (ThermoFisher Scientific) according to manufacturer's protocol, and the visualization was performed using a confocal laser scanning microscope (Leica SP5). For each complex, a xyz sequentially acquired images were captured using λ 488 laser to visualize the complexes and λ 633 laser for cell membrane visualization. Single plane and orthogonal projections of the z-stacks were evaluated for each complex internalization.

Cytotoxicity of the complexes

The cytotoxic effect of the complexes both in dark and light-activated samples was evaluated by the metabolic activity assay Alamar Blue (ThermoFisher Scientific). Complexes **1** and **2** were diluted as previously described and final concentrations of 5 µg/ml, 10 µg/ml, and 20

µg/ml were used for the experiments. A total amount of 50,000 SKBR-3 cells were seeded in 24 well-plates and cultured for 24 h. Then, different concentrations of the complex were added to the medium and cell were incubated for 4 h. After that, cells were irradiated using an 8 W lamp and a wavelength in the range 400-600 nm for 10 min. The metabolic activity of the cells was quantified after 48 h in culture using Alamar Blue assay, according to manufacturer's protocol. Samples containing the complexes in dark conditions were also evaluated. In both cases, cells cultured without complexes were used as controls for dark and light-activated conditions. The experiment was performed in triplicate.

Statistical analysis

The quantitative data were presented as the mean with the standard deviation. Statistical differences were evaluated using the one-way analysis of variance (ANOVA) with the Newman-Keuls multiple comparisons test. The analysis was performed using GraphPad Prism, and a p value of $p \leq 0.05$ was considered statistically significant.

ASSOCIATED CONTENT

The Supporting Information is available free of charge on the ACS Publications website.

Supplementary crystallographic information, spectroscopic characterization: NMR, UV-visible and ESI-MS spectra; additional electrochemical characterization and theoretical calculations.

AUTHOR INFORMATION

Corresponding Authors:

 *E-mail for I.R.: marisa.romero@udg.edu

*E-mail for R.N.: rosario@icmab.es

ORCID

Isabel Romero: 0000-0003-4805-8394

Rosario Núñez: 0000-0003-4582-5148

Carme Nogués: 0000-0002-6361-8559

Andreu Blanquer: 0000-0002-3551-1885

Xavier Fontrodona: 0000-0002-9873-1332

Zsolt Kelemen 0000-0002-4787-9804

NOTES

ACKNOWLEDGEMENTS

REFERENCES

[1] Lan M, Zhao S, Liu W, Lee C-S, Zhang W, Wang P. Photosensitizers for Photodynamic Therapy. Adv Healthcare Mater 2019;8:1900132.

[2] Kwiatkowski S, Knap B, Przystupski D, Saczko J, Kędzierska E, Knap-Czop K, Kotlińska J, Michel O, Kotowski K, Kulbacka J. Photodynamic therapy - mechanisms, photosensitizers and combinations. Biomed Pharmacother 2018;106:1098-1107.

[3] Kessel D, Oleinick N L. Photodynamic Therapy: Methods and Protocols, ed. C. J. Gomer, Human Press, Totowa, NJ, 2010, pp. 35-46. 12 K. Plaetzer, B. Krammer, J. Berland.

[4] Jiang J, Qian Y, Xu Z, Lv Z, Tao P, Xie M, Liu S, Huang W, Zhao Q. Enhancing singlet oxygen generation in semiconducting polymer nanoparticles through fluorescence resonance energy transfer for tumor treatment. Chem Sci 2019;10:5085-5094.

[5] Kamkaew A, Lim S H, Lee HB, Kiew L V, Chung L Y, Burgess K. BODIPY dyes in photodynamic therapy. Chem Soc Rev 2013;42:77-88.

[6] Turksoy A, Yildiz D, Akkaya, EU. Photosensitization and controlled photosensitization with BODIPY dyes. Coord Chem Rev 2019;379:47-64.

[7] Ortega-Forte E, Rovira A, Lopez-Corrales M, Hernandez-García A, Ballester FJ, Izquierdo-García E, Jordà-Redondo M, Bosch M, Nonell S, Santana MD, Ruiz J, Marchán V, Gasser G. A near-infrared light-activatable Ru (II)-coumarin photosensitizer active under hypoxic conditions. Chem Sci 2023;14:7170-7184.

[8] Lismont J, Dreesen L, Wuttke S. Metal-organic framework nanoparticles in photodynamic therapy: current status and perspectives. Adv Funct Mater 2017; 27:1606314.

[9] Liu J, Zhang C, Rees TW, Ke L, Ji L, Chao, H. Harnessing ruthenium (II) as photodynamic agents: Encouraging advances in cancer therapy. Coord Chem Rev 2018;363:17-28.

[10] Huang T, Yu Q, Liu S, Huang W, Zhao Q. Phosphorescent iridium(III) complexes: a versatile tool for biosensing and photodynamic therapy. Dalton Trans 2018;47:7628-7633.

[11] McKenzie LK, Bryant HE, Weinstein JA. Transition metal complexes as photosensitisers in one-and two-photon photodynamic therapy. Coord Chem Rev 2019;379:2-29.

[12] Poynton FE, Bright SA, Blasco S, Williams DC, Kelly JM, Gunnlaugsson T. The development of ruthenium (II) polypyridyl complexes and conjugates for in vitro cellular and in vivo applications. Chem Soc Rev 2017;46:7706-7756.

[13] Jin Z, Qi S, Guo X, Tian N, Hou Y, Li C, Wang X, Zhou Q. Smart use of "ping-pong" energy transfer to improve the two-photon photodynamic activity of an Ir (III) complex. Chem Commun 2020;56:2845-2848.

[14] Lang X, Zhao J, Chen X. Cooperative photoredox catalysis. Chem Soc Rev 2016;45: 3026–3038.

[15] Clerich E, Affès S, Anticó E, Fontrodona X, Teixidor F, Romero I. Molecular and supported ruthenium complexes as photoredox oxidation catalysts in water. Inorg Chem Front 2022;9:5347-5359.

[16] Hagfeldt A, Boschloo G, Sun L, Kloo L, Pettersson H. Dye-sensitized solar cells. Chem Rev 2010;110:6595-6663.

[17] Paul S, Kundu P, Kondaiah P, Chakravarty AR. BODIPY-Ruthenium(II) Bis-Terpyridine Complexes for Cellular Imaging and Type-I/-II Photodynamic Therapy. Inorg Chem 2021; 60:16178-16193.

[18] Lv Z, Wei H, Li Q, Su X, Liu S, Zhang KY, Lv W, Zhao Q, Li X, Huang W. Achieving efficient photodynamic therapy under both normoxia and hypoxia using cyclometalated Ru(II) photosensitizer through type I photochemical process. Chem Sci 2018;9:502-512.

[19] Conway-Kenny R, Ferrer-Ugalde A, Careta O, Cui X, Zhao J, Nogués C, Núñez R, Cabrera-González J, Draper SM. Ru(II) and Ir(III) phenanthroline-based photosensitisers bearing *o*-carborane: PDT agents with boron carriers for potential BNCT. Biomater. Sci. 2021;9:5691-5702.

[20] Conti L, Macedi E, Giorgi C, Valtancoli B, Fusi V. Combination of light and Ru(II) polypyridyl complexes: Recent advances in the development of new anticancer drugs. Coord Chem Rev 2022;15:214656.

[21] Conti L, Bencini A, Ferrante C, Gellini C, Paoli P, Parri M, Pietraperzia G, Valtancoli B, Giorgi C. Highly charged ruthenium (II) polypyridyl complexes as effective photosensitizer in photodynamic therapy. Chem Eur J 2019;25:10606−10615.

[22] Shum J, Leung PKK, Lo KKW. Luminescent ruthenium (II) polypyridine complexes for a wide variety of biomolecular and cellular applications. Inorg Chem 2019;58:2231-2247.

[23] Li A, Turro C, Kodanko JJ. Ru(II) polypyridyl complexes derived from tetradentate ancillary ligands for effective photocaging. Acc Chem Res 2018;51:1415-1421.

[24] Jakubaszek M, Goud B, Ferrari S, Gasser G. Mechanisms of action of Ru(II) polypyridyl complexes in living cells upon light irradiation. Chem Commun 2018;54:13040-13059.

[25] Karges J, Kuang S, Maschietto F, Blacque O, Ciofini I, Chao H, Gasser G. Rationally Designed Ruthenium Complexes for 1- and 2-Photon Photodynamic Therapy. Nat Commun2020;11(1):3262.

[26] Vinck R, Karges J, Tharaud M, Cariou K, Gasser G. Physical, spectroscopic, and biological properties of ruthenium and osmium photosensitizers bearing diversely substituted 4,4'-di(styryl)-2,2'-bipyridine ligands. Dalton Trans 2021;50:14629-14639.

[27] Li S, Zhao J, Wang X, Xu G, Gou S, Zhao Q. Design of a tris-heteroleptic Ru (II) complex with red-light excitation and remarkably improved photobiological activity. Inorg Chem 2020;59:11193-11204.

[28] Higgins SL, Brewer KJ. Designing red-light-activated multifunctional agents for the photodynamic therapy. Angew Chem Int Ed 2012;51:11420-1422.

[29] Rohrabaugh TN, Collins KA, Xue C, White JK, Kodanko JJ, Turro C. New Ru(II) complex for dual photochemotherapy: release of cathepsin K inhibitor and $^1O_2$ production. Dalton Trans 2018;47:11851-11858.

[30] Park H-J, Kim KH, Choi SY, Kim H-M, Lee WI, Kang YK, Chung YK. Unsymmetric Ru(II) Complexes with *N*-Heterocyclic Carbene and/or Terpyridine Ligands: Synthesis, Characterization, Ground- and Excited-State Electronic Structures and Their Application for DSSC Sensitizers. Inorg Chem 2010;49:7340-7352.

[31] Evans IP, Spencer A, Wilkinson G. Dichlorotetrakis (dimethyl sulphoxide) ruthenium (II) and its use as a source material for some new ruthenium (II) complexes. *J. Chem. Soc.*, Dalton Trans 1973;2:204-209.

[32] Halverson AP, Elmaaty TA, Castle LW. Complexes of (bpy)$_2$Ru(II) and (Ph$_2$bpy)$_2$Ru(II) with a series of thienophenanthroline ligands: synthesis, characterization, and electronic spectra. J Coord Chem 2011;64:3693-3699.

[33] Sens C, Rodríguez M, Romero I, Llobet A, Parella T, Benet-Buchholz J. Synthesis, Structure, and Acid-Base and Redox Properties of a Family of New Ru(II) Isomeric Complexes Containing the Trpy and the Dinucleating Hbpp Ligands. Inorg Chem 2003;42:8385-8394.

[34] Manrique E, Ferrer I, Lu C, Fontrodona X, Rodríguez M, Romero I. A Heterogeneous Ruthenium dmso Complex Supported onto Silica Particles as a Recyclable Catalyst for the Efficient Hydration of Nitriles in Aqueous Medium. Inorg Chem 2019;58:8460-8470.

[35] Caspar R, Cordier C, Waem JB, Guyard-Duhayon C, Gruselle M, Le Floch P, Amouri H. A New Family of Mono- and Dicarboxylic Ruthenium Complexes [Ru(DIP)$_2$(L$_2$)]$^{2+}$ (DIP = 4,7-diphenyl-1,10-phenanthroline): Synthesis, Solution Behavior, and X-ray Molecular Structure of *trans*-[Ru(DIP)$_2$(MeOH)$_2$][OTf]$_2$. Inorg Chem 2006;45:4071-4078.

[36] Balzani V, Juris A, Venturi M, Campagna S, Serroni S. Luminescent and redox-active polynuclear transition metal complexes. Chem Rev 1996;96:759-834.

[37] Rack JJ, Gray HB. Spectroscopy and Electrochemistry of *mer*-[RuCl$_3$(dmso)(tmen)]. Dimethylsulfoxide Is Sulfur-Bonded to Ru(II), Ru(III), and Ru(IV). Inorg Chem 1999;38:2-3.

[38] Teng Q, Huynh HV. A unified ligand electronic parameter based on ^{13}C NMR spectroscopy of N-heterocyclic carbene complexes. Dalton Trans 2017;46:614-627.

[39] Houten JV, Watts RJ. Temperature dependence of the photophysical and photochemical properties of the tris(2,2'-bipyridyl)ruthenium(II) ion in aqueous solution. Am Chem Soc 1976;98:4853-4858.

[40] Loftus LM, Al-Afyouni KF, Rohrabaugh TN, Gallucci Jr JC, Moore CE, Rack JJ, Turro C. Unexpected Role of Ru(II) Orbital and Spin Contribution on Photoinduced Ligand Exchange: New Mechanism To Access the Photodynamic Therapy Window. J Phys Chem C 2019;123:10291-10299.

[41] Loftus LM, Rack JJ, Turro C. Photoinduced ligand dissociation follows reverse energy gap law: nitrile photodissociation from low energy MLCT excited states. Chem Commun 2020;56:4070-4073.

[42] Suzuki K, Kobayashi A, Kaneko S, Takehira K, Yoshihara T, Ishida H, Shiina Y, Oishic S, Tobita S. Reevaluation of absolute luminescence quantum yields of standard solutions using a spectrometer with an integrating sphere and a back-thinned CCD detector. Phys Chem Chem Phys 2009;11:9850-9860.

[43] Zhang, Y.; Xu, Z.; Cai, L.; Lai, G.; Qiu, H.; Shen, Y. J. Photochem. Photobiol. A 2008, 200, 334– 345.

[44] Ferrer I, Rich J, Fontrodona X, Rodríguez M, Romero I. Ru (II) complexes containing dmso and pyrazolyl ligands as catalysts for nitrile hydration in environmentally friendly media. Dalton Trans 2013;42:13461-13469.

[45] Svensson FR, Li M, Nordén B, Lincoln P. Luminescent dipyridophenazine-ruthenium probes for liposome membranes. J Phys Chem B 2008;112:10969.

[46] Gill MR, Cecchin D, Walker MG, Mulla RS, Battaglia G, Smythe C, Thomas JA. Targeting the endoplasmic reticulum with a membrane interactive luminescent ruthenium(II) polypyridyl complex. Chem Sci 2013;4:4512-4519.

[47] Chen Q, Cuello-Garibo JA, Bretin L, Zhang L, Ramu V, Aydar Y, Batsiun Y, Bronkhorst S, Husiev Y, Beztsinna N, Chen L, Zhou XQ, Schmidt C, Ott I, Jager MJ, Brouwer AM, Snaar-Jagalska BE, Bonnet S. Photosubstitution in a trisheteroleptic ruthenium complex inhibits conjunctival melanoma growth in a zebrafish orthotopic xenograft model. Chem Sci 2022;13:6899-6919.

[48] Gründemann S, Kovacevic A, Albrecht M, Faller JW, Crabtree RH. Abnormal Ligand Binding and Reversible Ring Hydrogenation in the Reaction of Imidazolium Salts with $IrH_5(PPh_3)_2$. J Am Chem Soc 2002;124:10473-10481.

[49] APEX3 V2018 1-0. APX3 *v*2018 1-0. Bruker AXS 2018.

[50] SAINT V8.38A. Bruker AXS. SAINT V8.38A. Bruker AXS 2017.

[51] SADABS-2016/2 - Bruker AXS Area Detector Scaling andAbsorption Correction. SADABS-2016/2 - Bruker AXS área detector scaling and absorption correction.

[52] Sheldrick GM. A Short History of SHELX. Acta Crystallogr Sect A: Found. Crystallogr. 2008;64(1):112-122.

[53] Frisch MJ, Trucks GW, Schlegel HB, Scuseria GE, Robb MA, Cheeseman JR, Scalmani G, Barone V, Mennucci B, Petersson GA, Nakatsuji H, Caricato M, Li X, Hratchian HP, Izmaylov AF, Bloino J, Zheng G, Sonnenberg JL, Hada M, Ehara M, Toyota K, Fukuda R, Hasegawa J, Ishida M, Nakajima T, Honda Y, Kitao O, Nakai H, Vreven T, Montgomery JAJ, Peralta JE, Ogliaro F, Bearpark M, Heyd JJ, Brothers E, Kudin KN, Staroverov VN, Keith T, Kobayashi R, Normand J, Raghavachari K, Rendell A, Burant JC, Iyengar SS, Tomasi J, Cossi M, Rega N, Millam JM, Klene M, Knox JE, Cross JB, Bakken V, Adamo C, Jaramillo J, Gomperts R, Stratmann RE, Yazyev O, Austin AJ, Cammi R, Pomelli C, Ochterski JW, Martin RL, Morokuma K, Zakrzewski VG, Voth GA, Salvador P, Dannenberg JJ, Dapprich S, Daniels AD, Farkas O, Foresman JB, Ortiz JV, Cioslowski J, Fox DJ. Gaussian09, Revision E.01; Gaussian, Inc.: Wallingford, CT, 2013.

[54] Schaftenaar G, Nordik JH. Molden: a pre- and post-processing program for molecular and electronic structures. J Comput Aided Mol Des 2000;14:123-134.

[55] Gilbert ATB. IQmol molecular viewer. Available at: http://iqmol.org (Accessed October, 2012.

[56] O'Boyle NM, Tenderholt AL, Langner KM. Cclib: a library for package-independent computational chemistry algorithms. J Comp Chem 2008;29:839-845.

TOC GRAPHIC AND SYNOPSIS

A Ru(II) polypyridyl complex with three bulky 4,4'-diphenyl-2,2'-bipyridine ligands has proven to be a promising theranostic agent for bioimaging and PDT